Supplementary Information (SI) for Dalton Transactions.

Supporting information

Fabrication of a hierarchical PtIr@Rh hollow trimetallic nanozyme with a higher specific activity than HRP for sensitive colorimetric detection

Jincheng Yuan,[a] *Jian Hao,*[a] *Zeyang Yu,*[a] *Shengyang Hu,**[a] *Chenghui Zhai,*[a] *Jiawei Liu**[b] *and Kai Cai**[a]

[a] College of Chemistry & Environmental Engineering, Yangtze University, Jingzhou 434100, China. E-mail: shengyanghu@yangtzeu.edu.cn; caikai2000@163.com

[b] Key Laboratory of Earth and Planetary Physics, Institute of Geology and Geophysics, Innovation Academy for Earth Sciences, Chinese Academy of Sciences, Beijing 100029, China. E-mail: liujiawei@mail.iggcas.ac.cn

Materials and reagents.

All chemical reagents can be used without further purification after purchase. The following reagents were purchases from Aladdin Chemistry Co., Ltd.: Tellurium dioxide powder (TeO_2, 99.99%), and selenous acid (H_2SeO_3, 99.99%). The following reagents were purchases from Sinopharm Chemical Reagent Co., Ltd.: Hydrazine monohydrate ($N_2H_4 \cdot H_2O$, 85%, AR), sodium dodecyl sulfate (SDS, 99%), Chloroplatinic acid ($H_2PtCl_6 \cdot 6H_2O$, AR), Rhodium chloride hydrate ($RhCl_3 \cdot 3H_2O$), Iridic chloride ($IrCl_4$, AR), polyvinylpyr-rolidone (PVP10 Average molecular weight 58000 AR), hydrogen peroxide (H_2O_2, 30%, AR), and L-Ascorbic acid (AA, AR). The following reagents were purchases from McLean chemical reagent Co., Ltd.: 3,3',5,5'-tetramethylbenzidine (TMB), Citric acid/sodium (AR).

Instruments.

Transmission electron microscopy (TEM) imaging was conducted on a FEI TECNAI F30 microscope operated at 200 kV and copper grids were used to load the samples. All values of the material sizes were measured through TEM images. X-ray spectroscopy (EDS) was carried out under the high-angle annular dark field (HAADF) mode. Inductively coupled plasma-mass spectrometry (ICP-MS) measurements were performed on NexION 300Q (PerkinElmer, USA). X-ray diffraction (XRD) was tested on a Bruker D8 Advance X-ray diffractometer with Cu Kα radiation. Samples were prepared by depositing nanostructures on glass. The scanning speed was set as 15 degrees/min. X-ray photoelectron spectra (XPS) were collected on an ESCALAB 250Xi spectrophotometer (Thermo Fisher) with Al Kα X-ray radiation and calibrated using the C 1s peak (284.8 eV). UV-vis-NIR absorption spectra were measured by a Lambda 750UV-Vis-NIR spectrophoto meter (PerkinElmer, USA).

Debye–Scherrer equation.

$$D = \frac{k\lambda}{\beta cos\theta}$$

D is the grain size, k is the form factor, β is the full width at half maximum (FWHM) of the peak, θ is the angle of diffraction, and λ is the wavelength of the X-ray radiation.

Parameters in our work:

Peak	k	λ	2θ	θ	cosθ	FWHM (angle)	FWHM/β (radian)	D
(111)	0.89	0.154	40.029	20.014	0.940	1.434	0.025	5.829
(200)	0.89	0.154	46.524	23.262	0.919	1.456	0.025	5.874

Kinetic analysis.

Specifically, 0.1 M citric acid/sodium citrate were added successively as buffer (pH = 4.0). H_2O_2, nanozyme material (50 μL, 0.3 mg/L) and TMB were added in the cuvette (path length, l = 1.0 cm) at 20 °C. The final volume is controlled at 1 mL, in which the concentration of H_2O_2 is 2.0 M, and TMB is controlled as the variable. After adding all substances, the absorbance of the reaction solution at λ_{max} = 653 nm was measured by UV-vis spectrophotometer at an interval of 1 seconds for 50 s.

After obtaining the absorption-time curve, from which the initial reaction rate is calculated and the maximum reaction rate V_{max} and the Michaelis constant (K_m) are accessed by the Michaelis-Menten equation.

$$V = \frac{V_{max}[S]}{K_m + [S]}$$

where V_{max} is the maximal reaction velocity, [S] is the concentration of TMB, and K_m is the Michaelis constant. The values of K_m and V_{max} can be obtained from the double reciprocal plots.

Measurement of the Specific Activity.

Specifically, at 20 °C, 0.1 M citric acid/sodium citrate was selected as buffer (pH = 4.0). H_2O_2, nanozyme material, TMB (50 μL 10 mg/mL) were added successively. The final volume is controlled at 1 mL, in which the concentration of H_2O_2 is 1.0 M, and the quality of nanozyme material added each time is controlled. The absorbance of the reaction solution at λ_{max} = 653 nm was measured by UV-vis spectrophotometer at the interval of 1 second immediately after the addition of all substances for 50 s.

After obtaining the absorption-time curve, SA was calculated according to the formula below.

$$b_{nanozyme} = \frac{V}{\varepsilon l} \mathrm{X} \frac{\Delta A}{\Delta t}$$

where b_{nanozyme} is the nanozyme activity (U), V is the total volume of reaction solution (μL), ε is the molar absorption coefficient of the TMB substrate (39,000 M^{-1} cm^{-1} at 653 nm), l is the optical path length through reaction solution (cm), and ΔA/Δt is the initial rate of the absorbance change (min^{-1}). When using different amounts of the nanozyme to measure the peroxidase-like activity, the specific activity of the nanozyme was determined using the following equation:

$$SA = \frac{b_{nanozyme}}{m}$$

where SA is the specific activity of the nanozyme (U mg^{-1}), and m is the nanozyme amount (mg).

Free radical identification and quenching hydroxyl radical test.

The spin trap DMPO (100 mM) dissolved in deionized water was used as the work solution for hydroxyl radical (•OH) detection. Briefly, the analysis sample was freshly prepared by mixing PtIr@Rh HNRs (0.5 mg/L) and H_2O_2 (100 mM) in citric acid/sodium citrate buffer solution (0.1 M, pH = 4.0), followed by addition of work solutions and reacted for 5 min. The EPR spectrum was acquired for detection of spin adducts using spin traps.

Isopropanol is a commonly used hydroxyl radical quench agent that can quench hydroxyl radicals stably and reliably. By adding IPA to the reaction system, the reaction mechanism of nanozyme catalytic oxidation was investigated. The steps are as follows: In simple terms, 50 μL isopropanol, 50 μL TMB (10 mg/mL), 50 μL H_2O_2 with different concentrations and 50 μL nanozyme material (0.3 mg/L) were added to sodium citrate (0.1 M, pH = 4.0). The final volume is controlled at 1 mL, After adding all substances, the absorbance of the reaction solution at λ_{max} = 653 nm was measured by UV-vis spectrophotometer at an interval of 1 seconds for 50 s.

Density Functional Theory.

All DFT calculations were performed using the Vienna Ab initio Simulation Package

(VASP)[1]. The projector augmented wave (PAW)[2] pseudopotential with the PBE[3] generalized gradient approximation (GGA) exchange correlation function was utilized in the computations. The cutoff energy of the plane waves basis set was 500 eV and a Monkhorst-Pack mesh of 2×2×1 was used in K-sampling. All structures were spin polarized and all atoms were fully relaxed with the energy convergence tolerance of 10^{-4} eV per atom, and the final force on each atom was < 0.05 eV $Å^{-1}$.

Finally, the adsorption energies(E_{ads}) were calculated as $E_{ads} = E_{ad/sub} - E_{ad} - E_{sub}$, where $E_{ad/sub}$, E_{ad}, and E_{sub} are the total energies of the optimized adsorbate/substrate system, the adsorbate in the structure, and the clean substrate, respectively. The free energy was calculated using the equation:

$$G = E_{ads} + ZPE - TS$$

where G, E_{ads}, ZPE and TS are the free energy, total energy from DFT calculations, zero point energy and entropic contributions, respectively.

Colorimetric detection of AA.

The detection of AA was conducted as follows: 100 μL AA solutions of different concentrations, 50 μL H_2O_2 (0.4 M), 100 μL PtIr@Rh nanozyme (1 mg/L) and 50 μL TMB (10 mM) were added into a 2 mL tube containing 700 μL citric acid/sodium citrate buffer solution (0.1 M, pH = 4.0). After incubation for 5 min at room temperature, the absorption spectra were recorded in the range of 500−800 nm. All measurements were performed in triplicate, and the standard deviation was plotted as error bars.

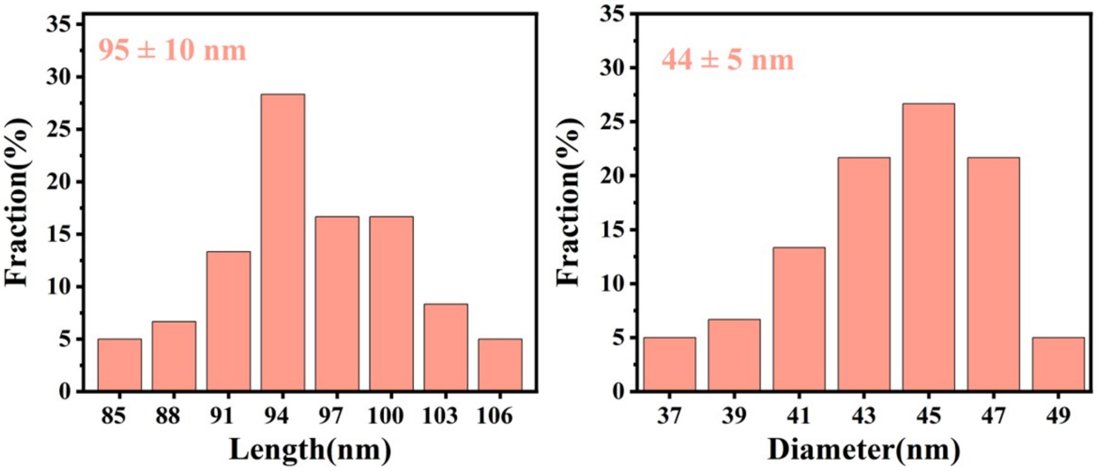

Figure S1 Length (A) and diameter (B) of PtIr@Rh nanorods.

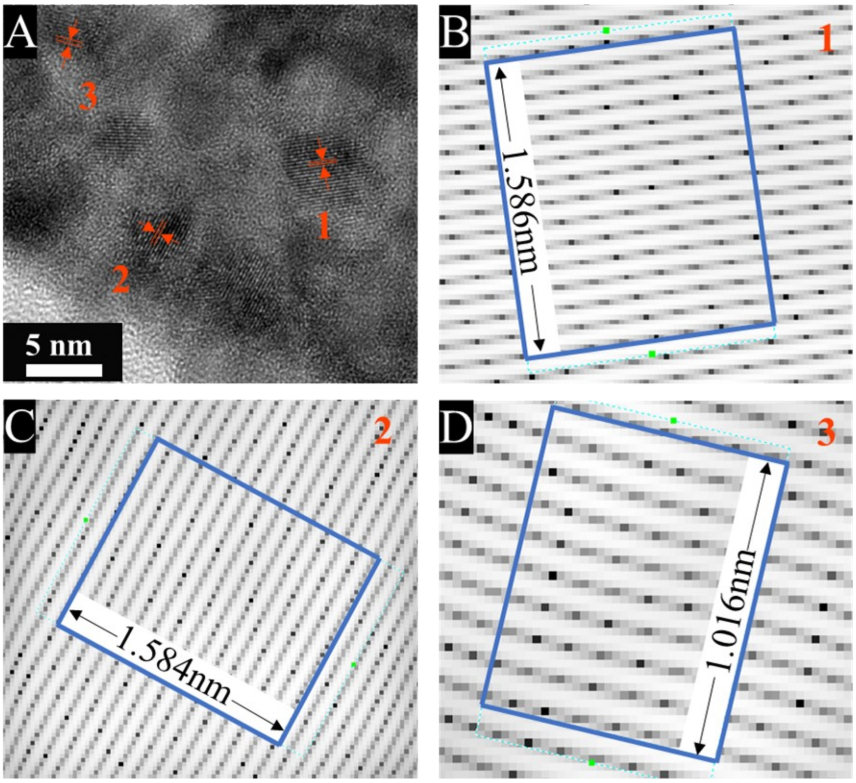

Figure S2 HRTEM image (A) and its corresponding inverse fast Fourier transform (IFFT) (B-D).

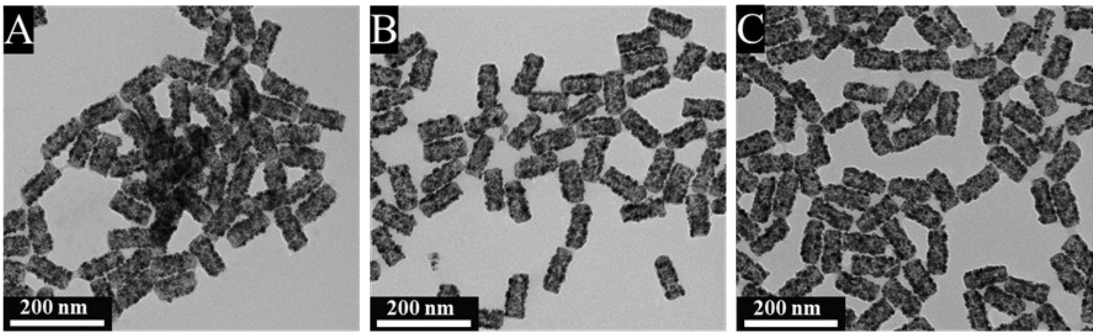

Figure S3 PtIr@Rh HNRs prepared with different concentrations of PVP. (A)1.0 mg PVP (B) 0.5 mg PVP (C) 0.1 mg PVP.

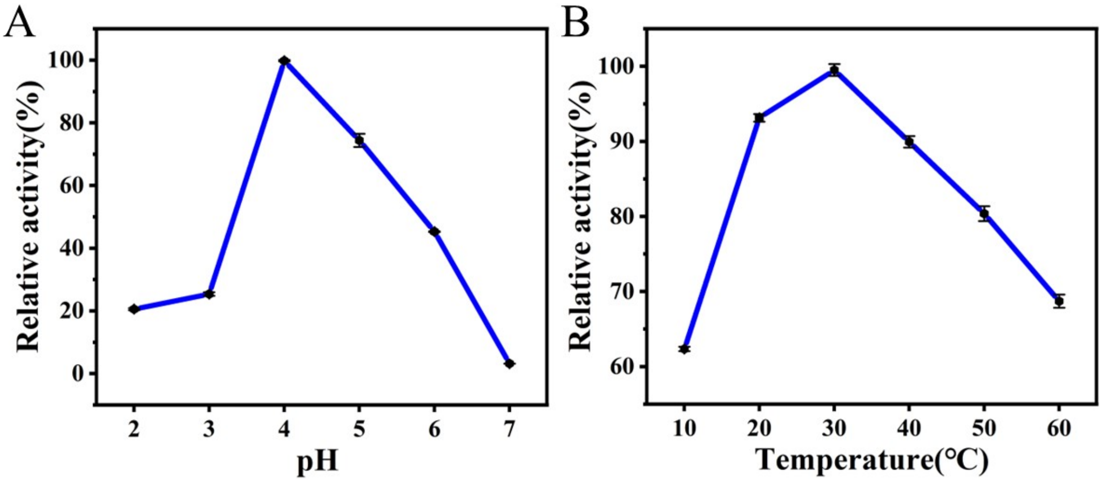

Figure S4. POD-like relative activities of PtIr@Rh nanozyme in different conditions. (A) different pH, (B) different temperature.

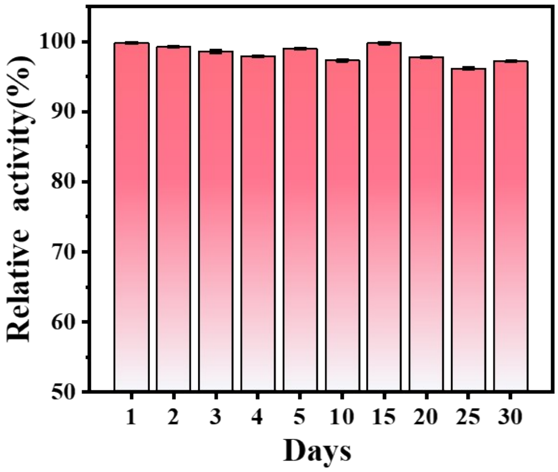

Figure S5. The stability of PtIr@Rh nanozyme. The maximum value is set as 100%.

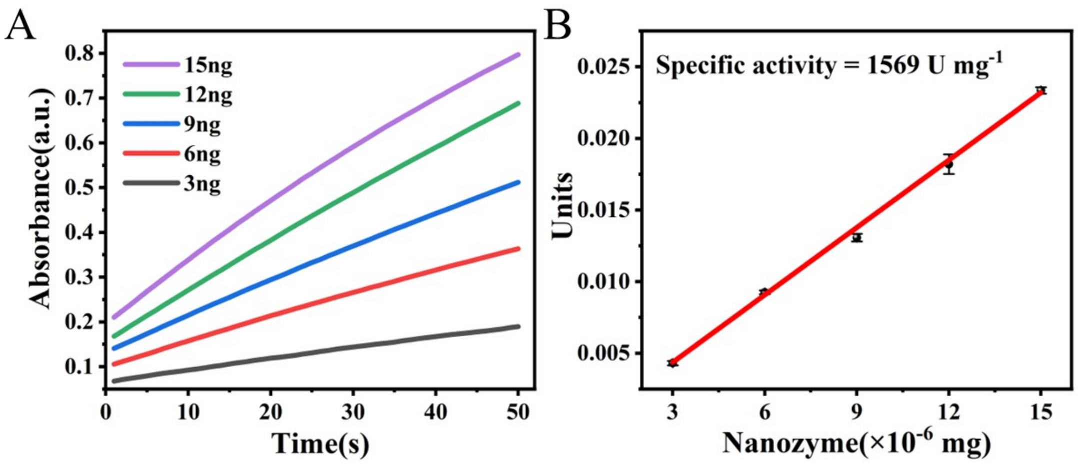

Figure S6. (A) Time-absorbance curves under different mass of PtIr@Rh-2 nanozyme. (B) Measurement of SA values of PtIr@Rh-2 nanozyme.

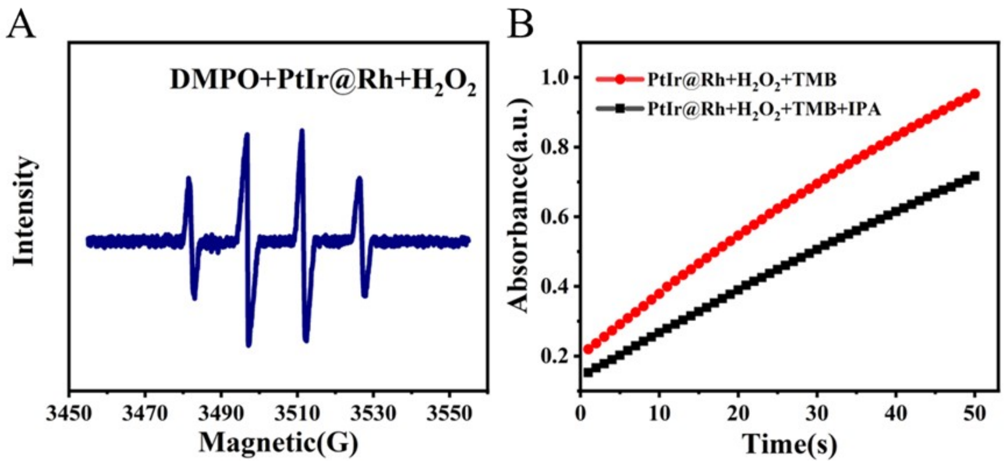

Figure S7. (A) EPR spectra of reaction systems using H_2O_2 and nanozyme at 5 min. (B) Time-absorbance curves of reaction systems with isopropanol (IPA) added or not under nanozyme.

Table S1 SA values of different nanozymes.

Nanozymes	SA (U mg^{-1})	Reference
A-Ru	164.46	4
Os NPs	393	5
PdPtAu alloys	81.245	6
AuPtCo	27.1	7
Pd-Ru NSs	59.01	8
Pd@Ir NSs	7.44	9
3.2 nm Pt NCs	13.5	10
Pt@CD	1877	11
HRP	208	12
HRP	297	13
HRP	507.5	14
HRP	267.7	15
Ru@PSS	2820	16
HRP	1305	
PtIr@Rh	2287	This work
PtIr@Rh-2	1569	

Table S2 Comparison of limits of detection of AA using different nanozymes.

Nanozymes	Detection range	Limit of detection	Reference
Pt-HMCNs	6.0-60μM	3.29μM	17
IrO2/GO	5-70μM	0.324μM	18
Au/Cu NRs	0-2 mM	25 μM	19
PtNi/NCFs	1-20 μM	0.94 μM	20
Hb-AuNPs	1-55μM	0.75μM	21
PVP-Pt NCs	2-50 μM	1.17 μM	22
Rh NSs	20-200 μM	6.63 μM	23
PdIr aerogels	0.5-250 μM	0.22 μM	24
Pd-Pt-Ir	25-800 μM	11.7μM	25
Pd-Pt-Ru	2-12μM	1.13μM	26
PtIr@Rh	0.5-45 μM	0.12μM	This work

References

[1] G. Kresse and J. Furthmüller, *Phys. Rev. B*, 1996, **54**, 11169-11186.

[2] P. E. Blöchl, *Phys. Rev. B*, 1994, **50**, 17953-17979.

[3] J. P. Perdew, K. Burke and M. Ernzerhof, *Phys. Rev. Lett.*, 1996, **77**, 3865-3868.

[4] Y. Tang, Y. Wu, W. Xu, L. Jiao, Y. Chen, M. Sha, H.-R. Ye, W. Gu and C. Zhu, *Anal. Chem.*, 2022, **94**, 1022-1028.

[5] S. He, L. Yang, P. Balasubramanian, S. Li, H. Peng, Y. Kuang, H. Deng and W. Chen, *J. Mater. Chem. A*, 2020, **8**, 25226-25234.

[6] L. Huang, Y. Zhou, Y. Zhu, H. Su, S. Yang, L. Feng, L. Zhao, S. Liu and K. Qian, *Biosens. Bioelectron.*, 2022, **210**, 114254.

[7] X. Zhou, C. Fan, Q. Tian, C. Han, Z. Yin, Z. Dong and S. Bi, *Anal. Chem.*, 2022, **94**, 847-855.

[8] J. Ming, T. Zhu, J. Li, Z. Ye, C. Shi, Z. Guo, J. Wang, X. Chen and N. Zheng, *Small*, 2021, **17**, 2103645.

[9] Z. Ye, Y. Fan, T. Zhu, D. Cao, X. Hu, S. Xiang, J. Li, Z. Guo, X. Chen and K. Tan, *ACS App. Mater. Interfaces*, 2022, **14**, 23194-23205.

[10] S. Chen, Z. Yu, Y. Wang, J. Tang, Y. Zeng, X. Liu and D. Tang, *Anal. Chem.*, 2023, **95**, 14494-14501.

[11] C. Liu, J. Hu, W. Yang, J. Shi, Y. Chen, X. Fan, W. Gao, L. Cheng, Q.-Y. Luo and M. Zhang, *Nanoscale*, 2024, **16**, 4637-4646.

[12] C. Chen, D. Yan, X. Jia, R. Li, L. Hu, X. Li, L. Jiao, C. Zhu, Y. Zhai and X. Lu, *Chem. Sci.*, 2024, **15**, 15440-15447.

[13] X. Niu, Q. Shi, W. Zhu, D. Liu, H. Tian, S. Fu, N. Cheng, S. Li, J. N. Smith, D. Du and Y. Lin, *Biosens. Bioelectron.*, 2019, **142**, 111495.

[14] N. Li, R. Li, Z. Li and X. Liu, *New J. Chem.*, 2024, **48**, 11407-11419.

[15] J. Wang, R. Gong, M. Yang, X. Wu, Z. Li, H. Huang, X. Yan and D. Wang, *Front. Chem.*, 2024, **12**, 1439039.

[16] H. Fan, J. Zheng, J. Xie, J. Liu, X. Gao, X. Yan, K. Fan and L. Gao, *Adv. Mater.*, 2024, **36**, 2300387.

[17] H. Chen, C. Yuan, X. Yang, X. Cheng, A. A. Elzatahry, A. Alghamdi, J. Su, X.

He and Y. Deng, *ACS Appl. Nano Mater.*, 2020, **3**, 4586-4598.

[18] H. Sun, X. Liu, X. Wang, Q. Han, C. Qi, Y. Li, C. Wang, Y. Chen and R. Yang, *Microchim. Acta*, 2020, **187**, 110.

[19] S. Xu, X. Dong, S. Chen, Y. Zhao, G. Shan, Y. Sun, Y. Chen and Y. Liu, *Sens. Actuators. B.*, 2019, **281**, 375-382.

[20] Y.-W. Mao, J.-Q. Li, R. Zhang, A.-J. Wang and J.-J. Feng, *ACS Appl. Nano Mater.*, 2023, **6**, 2805-2812.

[21] A. Kanwal, B. Saif, A. Muhammad, W. Liu, J. Liu, H. Ren, P. Yang and Z. Lei, *ACS Appl. Nano Mater.*, 2023, **6**, 4734-4746.

[22] X. Liu, M. Tian, C. Li and F. Tian, *Colloids Surf., A*, 2021, **625**, 126985.

[23] S. Cai, W. Xiao, H. Duan, X. Liang, C. Wang, R. Yang and Y. Li, *Nano Res.*, 2018, **11**, 6304-6315.

[24] X. Shi, J. Li, Y. Xiong, Z. Liu, J. Zhan and B. Cai, *Nanoscale*, 2023, **15**, 6629-6635.

[25] X. Tan, Q. Yang, X. Sun, P. Sun and H. Li, *ACS Appl. Mater. Interfaces*, 2022, **14**, 10047-10054.

[26] J. He, D. He, L. Yang, G.-L. Wu, J. Tian, Y. Liu and W. Wang, *Mater. Lett.*, 2022, **314**, 131851.

[27] J. He, L. Yang, Y. Zhang, R. Li, J. Wu, Q. Cao, S. Li, X. Wu, Y. Duan, D. He and W. Wang, *Anal. Methods*, 2023, **15**, 8-16.